Species-Independent Femtosecond Localized Electric Field Measurement

Arthur Dogariu,[1,*] Benjamin M. Goldberg,[1] Sean O'Byrne,[2] and Richard B. Miles[1]
[1]*Mechanical and Aerospace Engineering Department, Princeton University, Princeton, New Jersey 08544, USA*
[2]*School of Engineering and Information Technology, University of New South Wales Canberra, Campbell, Australian Capital Territory 2600, Australia*
(Received 11 April 2016; revised manuscript received 6 December 2016; published 23 February 2017)

We present an optical measurement method using a femtosecond laser for nonintrusive measurements of electric field strength and orientation in virtually any gas or gas mixture via second-harmonic generation. This simple method takes advantage of the asymmetry in polarizability induced by an applied electric field, which enables the otherwise forbidden second-harmonic generation in any centrosymmetric or homogeneous media. The use of a femtosecond laser source permits high intensities without avalanche breakdown and leads to the measurement of electric field strength down to approximately 100 V/cm in air with submillimeter spatial resolution governed by the confocal parameter and femtosecond temporal resolution governed by the laser-pulse duration.

DOI: 10.1103/PhysRevApplied.7.024024

I. INTRODUCTION

We present a nonintrusive optical method for the measurement of the local electric field in a gas with a high degree of spatial and temporal resolution. This method is based on second-harmonic generation through an electric-field-enabled nonresonant four-wave mixing interaction, which is localized within the Rayleigh range of the driving femtosecond pulsed laser beam. Two configurations are reported, one with a tightly focused laser for millimeter-scale localized measurements and the second with a more loosely focused laser to achieve higher sensitivity.

Three-wave nonlinear mixing processes such as second-harmonic generation are forbidden in symmetric and homogeneous media. An applied electric field breaks the symmetry and essentially converts the three-wave second-harmonic generation process into a four-wave mixing interaction leading to an output beam with intensity proportional to the square of the electric field. This nonresonant process allows for the measurement of electric fields in virtually any gas mixture by simply monitoring the amount of second-harmonic light generated. Femtosecond pulses achieve high light intensities without avalanche breakdown [1]. Since the second-harmonic output scales quadratically with the intensity of the driving laser, the high intensity associated with the femtosecond pulses leads to easily detected signals in gas mixtures such as air with electric field strengths as low as 100 V/cm. By calibrating the measurement method against a known set of electric field values, it is possible to take electric field measurements in highly transient field environments such as those typically found in nanosecond pulsed discharges.

Current state-of-the-art electric field measurement methods have successfully measured the electric field dynamics in plasmas using fluorescence from excited states of hydrogen [2] and Rydberg-states helium [3] as well as other atomic species, with the fluorescence dip technique. This method uses the Stark splitting of the excited-state transitions to determine the electric field. While permitting very precise electric field measurements to as low as a few volts per centimeter, the method is highly species dependent, requires narrow-linewidth lasers tuned to resonant transitions, and is limited to low pressures (approximately 1 Torr) where the Stark effect is apparent over any pressure-broadening effects. For nonintrusive electric field measurements at higher pressures, recent papers [4,5] have reported on the measurement of the electric field through a resonant four-wave mixing process similar to coherent anti-Stokes Raman scattering (CARS), where two driving lasers operate with wavelengths separated by the vibrational Raman shift of a gas molecule, and the applied electric field enables an otherwise forbidden coherent infrared transition producing an output infrared laser beam. This approach can also be modeled as a four-wave mixing process with one field being the applied field to be measured. In this case, the output power is linear with the product of the intensities of the two applied optical fields and quadratic with the electric field. This approach has been demonstrated for the measurement of electric fields in hydrogen producing an output beam at 2.4 μm [6] and in nitrogen producing an infrared beam at 4.29 μm [7]. While the CARS-like approach has the advantage of providing simultaneous visible CARS signals, which can be used for conventional CARS applications, it does require different driving laser wavelengths, as well as infrared detection at different wavelengths for each gas. Additionally, since it is a resonant technique, it does not

*adogariu@princeton.edu

work for atomic species and has been demonstrated only to be effective in H_2 and N_2 thus far.

The method presented here, femtosecond localized electric field measurement (FLEM), requires only a single laser which does not need to be resonant with any molecules, so measurements can be made in air and any other gas or gas mixtures including atomic gases. The output laser beam is in the visible wavelength range and is easily detected. The initial related work was done in the late 1960s and 1970s using nanosecond pulsed lasers [8]. The aim of those investigations was the determination of the nonlinear susceptibility of the gas with a known electric field, as opposed to determination of the electric field strength itself. Lasers such as the ruby, Nd:glass, and Nd:YAG laser with pulses much longer than tens of femtoseconds are limited in this application by avalanche ionization and associated gas breakdown and spark formation [1]. Thus, they achieve only very low signal levels at atmospheric pressures, and they cannot be focused tightly enough to measure local fields to millimeter scale.

The nonlinear susceptibility associated with electric-field-enabled second-harmonic generation (SHG) in gases was computed by Sitz and Yaris [9] in helium and by Kielich [10] in molecular gases. Measured electric-field-enabled second-harmonic signals in gases were recorded by Meyer [11] in air and other gases with both ruby and Nd:glass lasers and by Finn and Ward [12] with a ruby laser in noble gases. Bigio *et al.* [13] later used the electric-field-generated second harmonic with a localized electric field to measure the confocal beam parameter of a focused ruby laser. In the absence of an electric field, some second-harmonic light can be generated due to laser ionization and strong spatial laser-field gradients [14]. Recently, second-harmonic generation in air with no applied field has been enhanced with frequency-chirped femtosecond pulses [15] and tightly focused circular polarized femtosecond laser beams [16], which produce strong ponderomotive-driven local field gradients in laser-generated plasmas. Femtosecond second-harmonic generation has also been used for the detection of terahertz pulses [17].

The electric-field-enabled second-harmonic generation can be described as a third-order nonlinear process involving the light field and the applied electric field using the following expression [8]:

$$P_i^{(2\omega)} = \frac{3}{2} N \chi^{(3)}_{i,j,k,l}(-2\omega, 0, \omega, \omega) E_j^{(F)} E_k^{(\omega)} E_l^{(\omega)}, \quad (1)$$

where $P_i^{(2\omega)}$ is the induced polarization at 2ω, $E_{k,l}^{(\omega)}$ are the electric fields of the incident laser(s), which are both the same in second-harmonic generation, $E_j^{(F)}$ is the applied electric field, N is the number density of the molecular gas, and $\chi^{(3)}_{i,j,k,l}$ is the nonlinear susceptibility, which depends on the molecular dipole moments and field orientations [9]. The subscripts denote the polarizations of the respective fields. Note that even a time-varying electric field is seen as static by the femtosecond laser. The energy produced at the second harmonic is proportional to $\lceil P_i^{(2\omega)} \rceil^2$ times the interaction length squared plus a phase-matching factor [12], leading to a signal that is proportional to the square of the electric field strength and the square of the applied field intensity. There are two nonzero components of the susceptibility, $\chi^{(3)}_{y,y,y,y}$ and $\chi^{(3)}_{y,y,x,x}$, the first corresponding to the applied laser polarized parallel to the electric field and the second corresponding to the laser polarized perpendicular to the electric field. These components differ by a factor of 3 [18], leading to a factor of 9 change in the measured second-harmonic signal as the polarization of the laser is rotated relative to the electric field. This variation allows the measurement of the electric field direction. There is, in addition, a background of second-harmonic radiation that arises from the gradient of the driving laser and from laser-induced multiphoton ionization.

II. EXPERIMENTAL SETUP

The experimental apparatus is depicted in Fig. 1. The laser source is a Spectra-Physics Solstice Ace laser system, which produces 800-nm light with a pulse duration of 50 fs. Although the laser is capable of producing up to 6 mJ per pulse, a wave plate and polarizer are used to vary the energy up to a maximum of 0.5 mJ per pulse in order to avoid

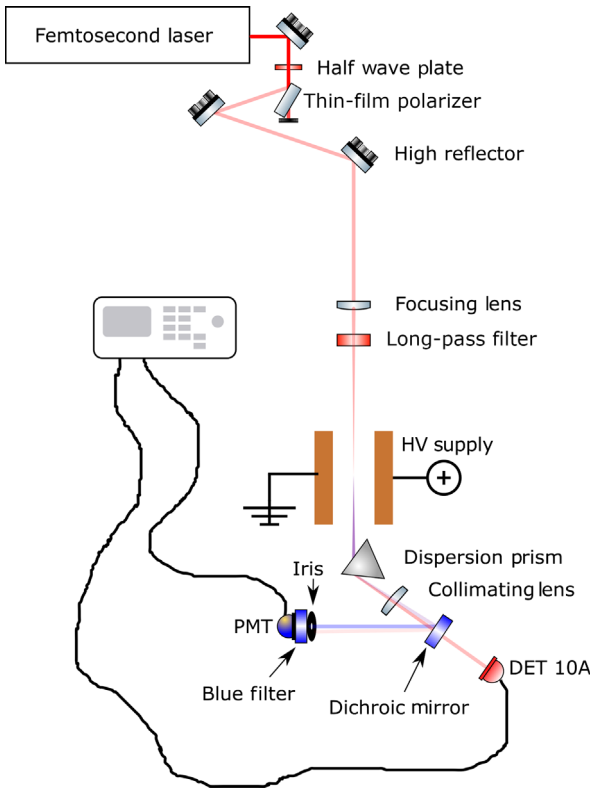

FIG. 1. FLEM experimental setup.

significant ionization in the interaction region. Initial experiments are conducted with the beam focused by a lens into a region of uniform electric field sustained between two parallel plates, 150 mm long and separated by 15 mm. The 400-nm light generated by the nonlinear interaction at the focus of the beam is spectrally separated from the fundamental 800-nm light using a single dispersion prism before being recollimated by a matched lens. The residual 800-nm light is filtered out by a series of short-wavelength pass and narrow-bandwidth filters placed in front of a photomultiplier tube, as well as an iris to block any scattered light from reaching the photomultiplier tube. To account for shot-to-shot fluctuations of the pump beam energy, a DET10A photodiode is used to collect and monitor the fundamental beam intensity after passing through the dichroic filter. Static electric field measurements are performed in a dc electric field provided by a variable high-voltage dc power supply, while time-varying results are obtained using a 20-ns rise time high-voltage switch pulser. Additionally, a half wave plate is used to rotate the polarization of the 800-nm light to measure the dependence of the signal on the relative polarizations of the laser and the electric field between the plates. Experiments are conducted in atmospheric pressure air using two focusing configurations; the first using a 3-m lens producing a focal zone 66 mm long (Rayleigh range) with a beam waist of 152 μm (FWHM) and a maximum peak intensity of 2×10^{12} W/cm^2 and the second using a 50-cm lens producing a focal zone 1.8 mm long, with a beam waist of 25 μm (FWHM) and a maximum peak intensity of 7×10^{13} W/cm^2. The first configuration produces stronger signals due to the longer interaction length, while the second, more tightly focused configuration, demonstrates a well-localized measurement capability. For the tight-focusing configuration in atmospheric pressure air, the zero-electric-field background signal is 16% of the 2 kV/cm dc electric-field-generated signal, whereas for the loose focusing at the same dc field strength, the zero-field background is 3.6% of the signal with the same 2 kV/cm electric field, indicating that for the tight-focusing case, some added background signal occurs due to the higher intensity and steeper laser-field gradients.

III. RESULTS AND DISCUSSION

Figure 2 shows the quadratic dependence predicted by Eq. (1) for the FLEM response as a function of the applied electric field in atmospheric pressure air collected with the 50-cm focusing geometry. A digital oscilloscope is used to collect individual waveforms for femtosecond pump beam intensity, second-harmonic beam intensity, applied voltage, as well as current measurements to ensure that no corona discharge from electrode edges occurs. The individual waveforms are then averaged in a postprocessing routine using bin sizes of approximately 50 V/cm. Varying the applied field results in several hundred laser shots collected

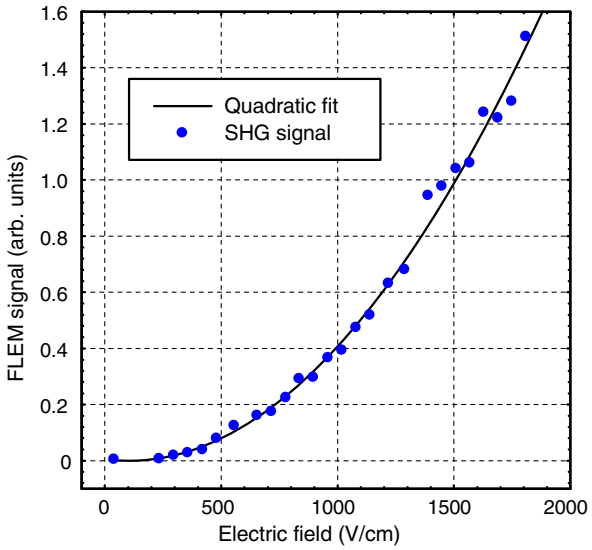

FIG. 2. Quadratic fit of the FLEM signal response with applied electric field. Data obtained in room air using 500 μJ per pulse and the $f = 50$ cm focusing geometry.

for each bin. Collecting and averaging individual laser shots allows for error analysis, with a measured standard deviation of approximately 20% of the mean second-harmonic signal value for each bin. Instabilities in the dc power supply are accounted for by measuring the applied voltage with a high-voltage probe. Using the given post-processing routine, a minimum sensitivity on the order of 200 V/cm is measured.

Because of the short sample time, FLEM has the capability to capture rapidly varying fields. To demonstrate this feature, high-voltage waveforms with a 20-ns rise time are generated using an in-house-built nanosecond pulser unit comprised of a Behlke HTS-151-02 high-voltage switch and associated control electronics. While the high-voltage switch is able to output pulses up to 15 kV with a rise time of approximately 20 ns, initial measurements are limited to 3-kV peak amplitude in order to ensure that the peak applied field is significantly below the breakdown threshold. Figure 3 shows the time response of the electric field measurement (symbols) compared with a single-waveform trace using a Tektronix P6015A high-voltage probe (solid line). Data are collected using the laser operating at 1 kHz as the master clock, which triggers a SRS DG535 delay generator set with a delay of approximately 1 ms to trigger the nanosecond pulser unit. It is necessary to trigger the pulser off the previous 1-ms-earlier laser pulse due to the long delay between when the nanosecond pulser is triggered and the high-voltage (HV) waveform is emitted. This long delay introduces a shot-to-shot jitter of approximately 10 ns between the laser and HV pulses to be measured. To compensate for this delay, individual high-voltage waveforms are saved on the digital oscilloscope, and the timing overlap with the laser pulse is analyzed in a postprocessing routine. For the data

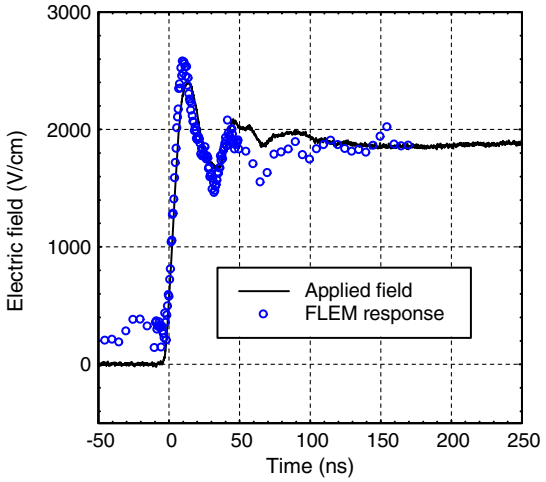

FIG. 3. High-voltage waveform with a voltage rise time of approximately 20 ns measured using FLEM. The FLEM calibration curve from Fig. 2 is used to determine the absolute applied electric field.

presented, time bins of 5 and 0.5 ns are used. It is important to emphasize that the femtosecond laser acts as a δ function when compared with the rate of change for the high-voltage waveform. Thus, the key limit on the temporal resolution of the measurement method is not the laser system itself but the resolution of the oscilloscope used to collect the data. For the data presented, a sampling frequency of 10 Gsample/ sec is used, allowing for accurate field measurements down to the hundreds of picoseconds.

Figure 4 shows the variation of the measured second-harmonic pulse energy as a function of the laser energy and polarization angle. In this case, the electric field is maintained constant at 2 kV/cm and the 3-m focusing geometry

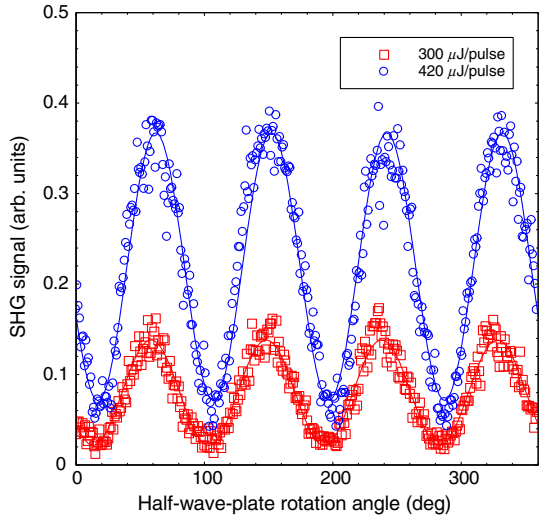

FIG. 4. Second-harmonic generation as a function of the half-wave-plate rotation angle for 300-μJ (red squares) and 420-μJ (blue circles) pulses focused to a 152-μm spot size (FWHM) in a uniform applied electric field of 2 kV/cm.

is used. The polarization of the input beam is rotated with the half wave plate, and the background nonelectric-field-related component is subtracted. The approximate factor of 9 variation due to polarization is apparent. The peaks in these data align with the electric field and clearly indicate its direction. The two curves shown are obtained using different laser-pulse energies, 300 μJ (squares) and 420 μJ (circles), highlighting the better sensitivity of the measurement method with increased fundamental laser-pulse energy. The magnitude of the signals in Fig. 4 also shows the quadratic dependence of the measured signal with the laser input intensity predicted by Eq. (1). The ratio of the SHG signals shown in Fig. 4 is 2.5, which, according to the quadratic dependence predicted by Eq. (1), corresponds to a measured intensity ratio of 1.58, very close to the actual 1.5 ratio between the laser energies used for the two measurements.

The ability to obtain localized field measurements depends upon the optical measurement volume following the Rayleigh range of the focusing optics. To demonstrate this, an experiment is set up where a pin electrode with a head diameter of 1.6 mm is scanned along the beam's propagation axis over a flat, grounded electrode. The electric field is kept below 4 kV/cm in order to avoid a corona discharge. Figure 5(a) shows the measured second-harmonic response as a function of the pin electrode position with respect to the focused beam waist (located at $x = 0$) for focal lengths of 75, 50, 30, and 15 cm. The spatial resolution of the FLEM can be estimated from measuring the spatial extent of the SHG signal as a function of the Rayleigh range [the fits in Fig. 5(a) assume Gaussian propagation]. The beam-focusing parameter is measured each time accurately by performing Z-scan experiments [19], where the two-photon absorption is monitored while scanning a thin ZnSe crystal through the focal region. Figure 5(b) shows that the measurement volume follows the Rayleigh range down to the radial extent of the electric field, which is estimated to be approximately 2 mm in the area where the beam is focused. This means that one can obtain accurate local measurements of the field, spatially limited only by the beam-focusing parameters, which is submillimeter for tight focusing.

The utility of this approach for the single-shot measurement of the local electric field depends on the signal-to-noise ratio, which, in turn, depends on the electric field strength and the laser-focusing geometry. Figure 6 shows 100 individual second-harmonic pulse amplitudes on a logarithmic scale for both loose- and tight-focus configurations at field strengths held constant at 700, 2000, and 3900 V/cm. The larger scatter at 700 and 2000 V/cm corresponds to the tight-focusing geometry and correlates with the weaker signals detected in that geometry. The data at 3900 V/cm are from the tight-focusing geometry, and at this field strength, the shot-to-shot uncertainty is approximately 20%. These data are merged with 100 pulse-averaged data for other voltages and from both focusing geometries in

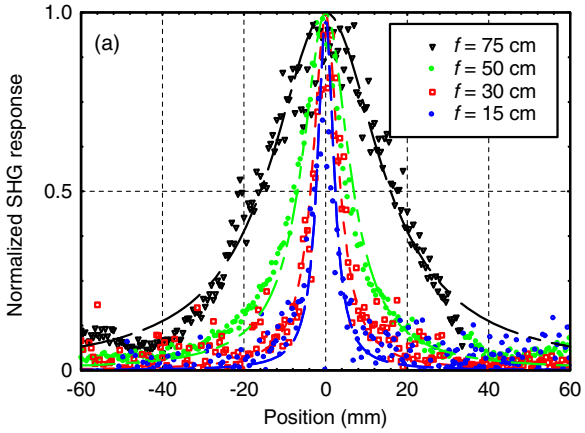

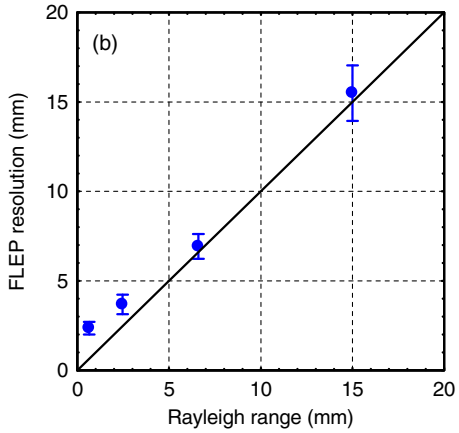

FIG. 5. Spatial resolution of FLEM measured as the spatial extend of the SHG signal assuming Gaussian propagation fits (a) follow the Rayleigh range of the beam-focusing geometry (b), as indicated by Z-scan measurements, allowing for accurate measurement high spatial resolution.

atmospheric pressure air in Fig. 7, where the quadratic scaling of the signal with electric field strength can be seen, along with the uncertainty (variance) for the loose focusing (circles) and the tight focusing (squares). Note that for the loose focusing, good data are achieved to well below 1000 V/cm, and measurable signals are seen down to 100 V/cm.

Thus, depending on the electric field distribution, one can use a focusing geometry which gives the best results: achieving electric field measurements with high sensitivity (the loose-focusing geometry) for electric fields as low as 100 V/cm or measuring higher-strength electric fields with very high spatial resolution (the tight-focusing geometry). Additionally, it can be seen from Fig. 7 that the quadratic fit with electric field is maintained regardless of the beam-focusing geometry. Because of the index mismatch between the fundamental and the second harmonic and coherent interference with the background SHG, the signals measured under a different focusing configuration cannot be directly compared, and, hence, calibration curves such as the ones shown in Figs. 1 and 7 have to be performed for absolute electric field measurements.

This approach to the measurement of electric fields by the generation of the second harmonic is nonresonant, so it can be used to measure electric fields in any gas or gas mixture without changing the laser or detection wavelengths. Electric fields have been measured in a variety of gases including air, Ar, H_2, N_2, CH_4, and CO_2, without any changes in the experimental configuration.

Figure 8 shows a set of normalized calibration curves measured for each of the different gases. The data shown in Fig. 8 are collected in the single-shot mode described previously using the tight-focusing geometry and with 500-μJ pump pulses. The electric field test cell is vacuumed and flushed several times with the gas to be examined and then filled to a pressure of 780 Torr in order to ensure that no ambient air leaks into the cell. For all gasses tested, a second-harmonic signal is readily detectable, and a

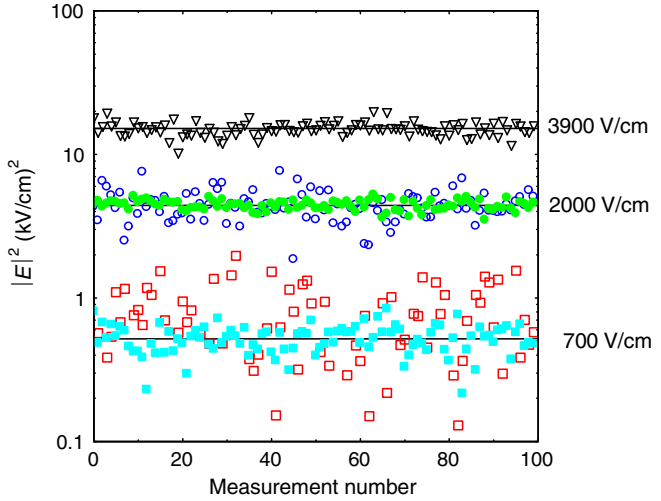

FIG. 6. Signal fluctuation for $E = 700$ V/cm (squares), 2000 V/cm (circles), and 3900 V/cm (triangles), while focusing to achieve a spatial resolution of 1.8 mm (open markers) and 66 mm (solid markers).

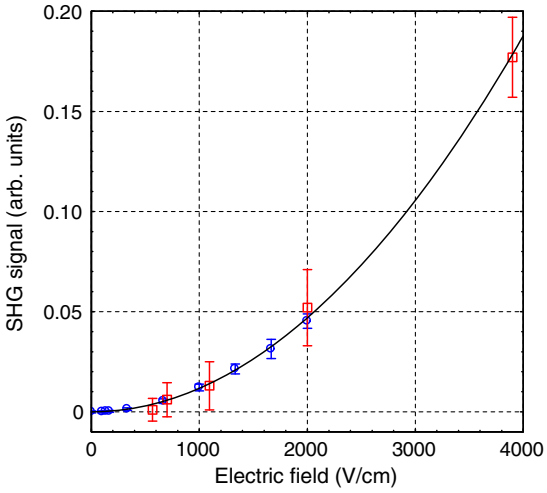

FIG. 7. Quadratic dependence of SHG on the electric field applied measured while focusing the pump laser to 25 μm (circles), and 152 μm (squares), with a spatial resolution of 66 and 1.8 mm, respectively.

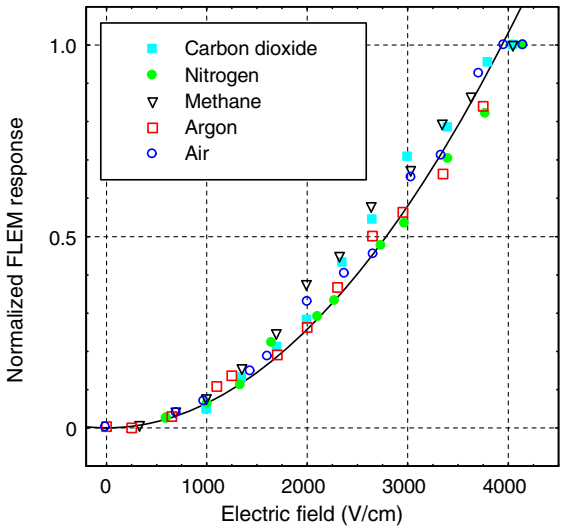

FIG. 8. Normalized quadratic calibration curves for several different species. For all gases tested, second-harmonic signals are readily detectable, and the standard deviation of the means do not exceed 20% of the mean values.

standard deviation of the mean error analysis is approximately 20% of the mean signal at each field value, consistent with results presented above. The data in Fig. 8 are normalized to account for the different susceptibility of each gas and for the index of refraction mismatch between the fundamental and second-harmonic wavelengths. The quadratic fit provides a calibration which is required for each gas for electric field measurements. The signals obtained in different gases depend on the hyperpolarizability as predicted by Eq. (1), and FLEM can be used to compare the nonlinear response of gases, provided that the interaction region given by the focal parameter is much smaller than the second-harmonic process coherence length.

IV. CONCLUSION

In conclusion, a simple method for the measurement of electric fields in air and other gas mixtures is presented based on the detection of second-harmonic generation at a selected location by using a focused femtosecond laser beam. The method is purely optical, can be applied *in situ*, and can accurately sample the electric fields with very high spatial (submillimeter) and temporal (subpicosecond) resolution. The high temporal resolution provided by the use of femtosecond pulses makes this method very appealing for characterizing transient electric fields such as those obtained using subnanosecond pulsers.

ACKNOWLEDGMENTS

We gratefully acknowledge the financial support from the Army Research Office Grant No. W911NF-15-1-0236 under Dr. Matthew Munson.

[1] M. N. Shneider and R. B. Miles, Laser induced avalanche ionization in gases or gas mixtures with resonantly enhanced multiphoton ionization or femtosecond laser pulse pre-ionization, Phys. Plasmas **19**, 083508 (2012).

[2] U. Czarnetzki, D. Luggenhölscher, and H. F. Döbele, Sensitive Electric Field Measurement by Fluorescence-Dip Spectroscopy of Rydberg States of Atomic Hydrogen, Phys. Rev. Lett. **81**, 4592 (1998).

[3] U. Czarnetzki, D. Luggenhölscher, and H. F. Döbele, Investigations on ionic processes and dynamics in the sheath region of helium and hydrogen discharges by laser spectroscopic electric field measurements, Appl. Phys. A **72**, 509 (2001).

[4] V. P. Gavrilenko, E. B. Kupriyanova, D. P. Okolokulak, V. N. Ochkin, S. Yu. Savinov, S. N. Tskhai, and A. N. Yarashev, Generation of coherent IR light on a dipole-forbidden molecular transition with biharmonic pumping in a static electric, JETP Lett. **56**, 1 (1992).

[5] B. Goldberg, I. Shkurenkov, S. O'Byrne, I. Adamovich, and W. Lempert, Electric field vector measurements in a surface ionization wave discharge, Plasma Sources Sci. Technol. **24**, 035010 (2015).

[6] D. A. Akimov, A. M. Zheltikov, N. I. Koroteev, A. N. Naumov, A. Y. Serdyuchenko, S. A. Sidorov-Biryukov, A. B. Fedotov, V. N. Ochkin, and S. N. Tskhai, Coherent Raman scattering in molecular hydrogen in a dc electric field, JETP Lett. **70**, 375 (1999).

[7] T. Ito, K. Kobayashi, S. Mueller, D. Luggenhölscher, U. Czarnetzki, and S. Hamaguchi, Electric field measurement in an atmospheric or higher pressure gas by coherent Raman scattering of nitrogen, J. Phys. D **42**, 092003 (2009).

[8] J. F. Ward and I. J. Bigio, Molecular second- and third-order polarizabilities from measurements of second-harmonic generation in gases, Phys. Rev. A **11**, 60 (1975).

[9] P. Sitz and R. Yaris, Frequency dependence of the higher susceptibilities, J. Chem. Phys. **49**, 3546 (1968).

[10] S. Kielich, Optical harmonic generation and laser light frequency mixing processes in nonlinear media, Optoelectronics, Instrumentation and Data Processing **2**, 125 (1970).

[11] G. Mayer, Rayonnement de l'harmonique pair d'une onde lumineuse par des molècules soumises à un champ èlectrique statique, C.R. Acad. Sci (Paris) **267B**, 54 (1968).

[12] R. S. Finn and J. F. Ward, dc-Induced Optical Second-Harmonic Generation in the Inert Gases, Phys. Rev. Lett. **26**, 285 (1971).

[13] I. J. Bigio, R. S. Finn, and J. F. Ward, Electric-field induced harmonic generation as a probe of the focal region of a laser beam, Appl. Opt. **14**, 336 (1975).

[14] D. S. Bethune, Optical second harmonic generation in atomic vapors with focused beams, Phys. Rev. A **23**, 3139 (1981); **25**, 2845(E) (1982).

[15] G. Li, J. Ni, H. Xie, B. Zeng, J. Yao, W. Chu, H. Zhang, C. Jing, F. He, H. Xu, Y. Cheng, and Z. Xu, Second harmonic generation in centrosymmetric gas with spatiotemporally focused intense femtosecond laser pulses, Opt. Lett. **39**, 961 (2014).

[16] M. Beresna, P. G. Kazansky, Y. Svirko, M. Barkauskas, and R. Danielius, High average power second harmonic generation in air, Appl. Phys. Lett. **95**, 121502 (2009).

[17] J. Dai, X. Xie, and X.-C. Zhang, Detection of Broadband Terahertz Waves with a Laser-Induced Plasma in Gases, Phys. Rev. Lett. **97**, 103903 (2006).

[18] I. J. Bigio and J. F. Ward, Measurement of the hyperpolarizability ratio $X_{yyyy}(-2\omega;0,\omega,\omega)/X_{yyxx}(-2\omega;0,\omega,\omega)$ for the inert gases, Phys. Rev. A **9**, 35 (1974).

[19] M. Sheik-Bahae, A. A. Said, T. H. Wei, D. J. Hagan, and E. W. Van Stryland, Sensitive measurement of optical nonlinearities using a single beam, IEEE J. Quantum Electron. **26**, 760 (1990).